REPORT

Form Approved
OMB No. 0704-0188

1. Agency Use Only *(Leave blank)*

1989

and Dates Covered.
Journal Article

4. Title and Subtitle.
A parabolic equation model for scattering in the ocean

5. Funding Numbers.
Program Element No. 61153N
Project No. 3202
Task No. OH0
Accession No. DN257015

6. Author(s).
Michael D. Collins and Michael F. Werby

7. Performing Organization Name(s) and Address(es).
Naval Oceanographic and Atmospheric Research Laboratory*
Stennis Space Center, MS 39529-5004

8. Performing Organization Report Number.
JA 224:085:88

9. Sponsoring/Monitoring Agency Name(s) and Address(es).
Naval Oceanographic and Atmospheric Research Laboratory*
Stennis Space Center, MS 39529-5004

10. Sponsoring/Monitoring Agency Report Number.
JA 224:085:88

11. Supplementary Notes.
*Formerly Naval Ocean Research and Development Activity
J. Acoust. Soc. Am.

12a. Distribution/Availability Statement.
Approved for public release; distribution is unlimited.

12b. Distribution Code.

13. Abstract *(Maximum 200 words)*.
The small-angle-of-propagation limit and the method of matched asymptotics are applied to derive an efficient model for solving realistic underwater acoustics problems involving both propagation and scattering from a submerged object. the propagation and scattering aspects of the waveguide scattering problem are decoupled by approximating the waveguide Green's function on the surface of the scatterer. For low frequencies, the small-angle limit also allows one to approximate the incident field with a horizontally propagating plane wave and the scattered field with an azimuthally specular point-source field. With these approximations, scattering calculations can be performed efficiently in the time domain. Calculations involving the three-dimensional parabolic equation and the time-domain parabolic equation are presented.

14. Subject Terms.
(U) Transients; (U) Distributed Sensors; (U) Coherence; (U) Detection, (U) Classification

15. Number of Pages.
8

16. Price Code.

17. Security Classification of Report.	18. Security Classification of This Page.	19. Security Classification of Abstract.	20. Limitation of Abstract.
Unclassified	Unclassified	Unclassified	SAR

A parabolic equation model for scattering in the ocean

Michael D. Collins and Michael F. Werby
Naval Ocean Research and Development Activity, Stennis Space Center, Mississippi 39529

(Received 20 July 1988; accepted for publication 18 January 1989)

The small-angle-of-propagation limit and the method of matched asymptotics are applied to derive an efficient model for solving realistic underwater acoustics problems involving both propagation and scattering from a submerged object. The propagation and scattering aspects of the waveguide scattering problem are decoupled by approximating the waveguide Green's function on the surface of the scatterer. For low frequencies, the small-angle limit also allows one to approximate the incident field with a horizontally propagating plane wave and the scattered field with an azimuthally specular point-source field. With these approximations, scattering calculations can be performed efficiently in the time domain. Calculations involving the three-dimensional parabolic equation and the time-domain parabolic equation are presented.

PACS numbers: 43.30.Gv, 43.30.Bp, 43.30.Dr

INTRODUCTION

Several models have been developed for solving problems in both underwater propagation[1] and free-space scattering.[2] Yet these remain highly active areas of research. Thus it is not surprising that model development for scattering in a waveguide, a problem involving both propagation and scattering, has only recently begun. The few models that have been developed[3-5] do not take advantage of asymptotic limits. Thus these models lack both simplicity and efficiency and are difficult to apply to realistic problems.

The small-angle limit (nearly horizontal rays) is perhaps the most useful asymptotic limit in underwater acoustics. This limit is used to derive the parabolic equation (PE),[6] which gives accurate and efficient results for propagation problems in complicated ocean environments. The three-dimensional PE (3DPE)[7-9] is required in general. However, the two-dimensional PE (2DPE) is valid whenever azimuthal diffraction is negligible.[10] The inverse Fourier transform is applied to the PE to derive the time-domain PE (TDPE),[11-16] which is an accurate and efficient pulse propagation model. If the source and receiver are sufficiently far from the scatterer, these models can be used to propagate the incident field to the scatterer and the scattered field to the receiver.

For a point source, the nearfield effects of attenuation and variations in sound speed and density do not affect the farfield.[17] Since a scatterer behaves like a source, this suggests that the far waveguide scattered field is not affected by refraction, reflection, and dissipation near the scatterer. We demonstrate this using the results of Ref. 17 and the method of matched asymptotics.[18] We show that the scattering and propagation aspects of the waveguide scattering problem decouple into the homogeneous half-space scattering problem and simple propagation problems.

The half-space scattering problem is further simplified for low frequencies using the small-angle limit. The incident field can be approximated by a plane wave, and the scattered field can be approximated by the field due to an azimuthally specular point source. These approximations allow efficient pulse scattering calculations. Scattering calculations involving the TDPE and the 3DPE are presented.

I. THE FARFIELD APPROXIMATION

Cylindrical coordinates are used with z being the depth below the ocean surface, θ being the azimuth angle, and r being the horizontal distance from the center of the scatterer Γ of length L at $z = z_0$. The point source Ω is located at $(r,z,\theta) = (r_s,z_s,\theta_s)$. The coordinate system and geometry are illustrated in Fig. 1. The ocean depth is denoted by d. The acoustic pressure p satisfies the pressure release boundary condition at the ocean surface and the outgoing radiation condition at infinity. For the time-harmonic problem with circular frequency ω, the complex pressure P is defined by

$$p(r,z,\theta,t) = P(r,z,\theta)\exp(-i\omega t), \tag{1}$$

where t is time. Away from Γ and Ω, P is assumed to satisfy the reduced wave equation for a medium with variable density[19]

$$\rho\nabla\cdot[(1/\rho)\nabla P] + K^2 P = 0, \tag{2}$$

where ρ is the density and the complex wavenumber $K = k + i\eta\beta k^2$ is used to model attenuation that depends linearly on frequency.[20] The real wavenumber is $k = \omega/c$, where c is the sound speed. The reference wavenumber is $k_0 = k(z_0)$, the reference sound speed is $c_0 = c(z_0)$, the sediment attenuation in decibels per wavelength (dB/λ) is β, and $\eta = (40\pi\log_{10} e)^{-1}$.

Rays that propagate within the critical angle ϕ_c from horizontal are called trapped rays. We define $\epsilon = \tan^2\phi_c$ and assume that $\epsilon \ll 1$. The critical range r_c, which is defined by $r_c \tan\phi_c = d - z_0$, is the range at which the steepest trapped ray from the center of Γ intersects the ocean bottom. To justify using the PE approximation, we assume that range and azimuth variations in the environment are weak. The incident field P_i is defined to be the field due to Ω in the absence of Γ, and the scattered field P_s is defined by $P = P_i + P_s$. The waveguide Green's function $G(\mathbf{x},\mathbf{x}')$ satisfies the pressure release boundary condition at the ocean surface, the outgoing radiation condition at infinity, and

 0001-4966/89/051895-08$00.80

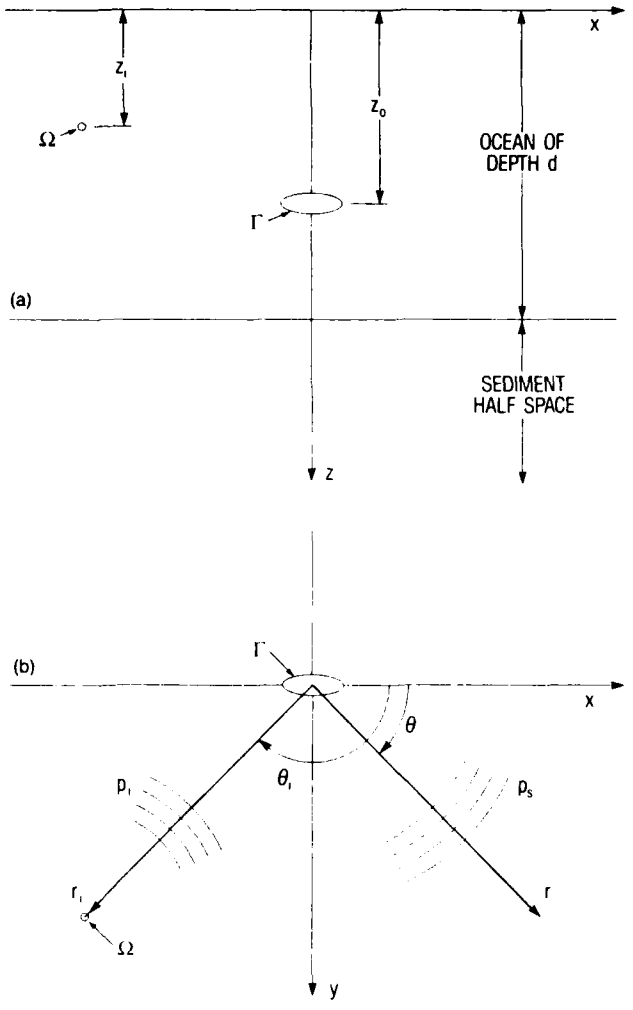

FIG. 1. Coordinate systems and geometry: (a) View from the side; (b) view from above the ocean surface.

$$\rho\nabla\cdot[(1/\rho)\nabla G] + K^2 G = -4\pi\delta(\mathbf{x}-\mathbf{x}'), \tag{3}$$

$$\mathbf{x} = (x,y,z) = (r\cos\theta, r\sin\theta, z). \tag{4}$$

Our definition of G differs from the usual definition of the Green's function by a factor of 4π. The scattered field has the representation

$$P_s(\mathbf{x}) = \frac{1}{4\pi}\int\int_{\partial\Gamma}\left(\frac{\partial G}{\partial n}(\mathbf{x},\mathbf{x}')P(\mathbf{x}') - \frac{\partial P}{\partial n}(\mathbf{x}')G(\mathbf{x},\mathbf{x}')\right)dA', \tag{5}$$

where $\partial/\partial n$ is the outward normal derivative, G is the field due to a point source at $\mathbf{x} = \mathbf{x}'$, and $\partial G/\partial n$ can be approximated with arbitrary accuracy by a pair of point sources near $\mathbf{x} = \mathbf{x}'$. Thus P_s can be approximated with arbitrary accuracy as the field due to a superposition of point sources on and near $\partial\Gamma$.

In the homogeneous free space with $c = c_0$ and $\beta = 0$, the integral representation can be used to obtain the following farfield expansion for the free-space scattered field $(P_s)_f$ for an incident plane wave of unit amplitude[21]

$$(P_s)_f(\mathbf{x}) \sim D_f(\theta,\phi)G_f(\mathbf{x},\mathbf{x}_0), \tag{6}$$

$$G_f(\mathbf{x},\mathbf{x}') = [\exp(ik_0|\mathbf{x}-\mathbf{x}'|)]/|\mathbf{x}-\mathbf{x}'|, \tag{7}$$

$$\mathbf{x}_0 = (0,0,z_0), \tag{8}$$

$$\phi = \tan^{-1}[(z-z_0)/r]. \tag{9}$$

For large r, $\partial H/\partial r = O(k_0\epsilon)$, $\partial H/\partial z = O(k_0\epsilon^{1/2})$, and $\partial H/\partial\theta \ll k_0 r$ (Ref. 8). For the case $k_0 L = O(1)$, the weakly varying coefficient function $H(\mathbf{x},\mathbf{x}')$ can be replaced by the constant $H(\mathbf{x},\mathbf{x}_0)$ for $\mathbf{x}' \in \partial\Gamma$ to leading order in ϵ. With this approximation, the integrand in Eq. (5) is reduced to a form in which the analysis of Ref. 21 can be applied for $r \gg L$. We obtain

$$\sqrt{(x-x')^2 + (y-y')^2} \cong r - \mathbf{x}'\cdot\hat{r}, \tag{11}$$

$$G(\mathbf{x},\mathbf{x}') \cong G(\mathbf{x},\mathbf{x}_0)\exp(-ik_0\mathbf{x}'\cdot\hat{r}), \tag{12}$$

$$\frac{\partial G}{\partial n}(\mathbf{x},\mathbf{x}') \cong -ik_0\hat{n}\cdot\hat{r}G(\mathbf{x},\mathbf{x}_0)\exp(-ik_0\mathbf{x}'\cdot\hat{r}), \tag{13}$$

where $\hat{r} = (\cos\theta, \sin\theta, 0)$ and $\hat{n}$ is the outward normal unit vector on $\partial\Gamma$. Substituting Eqs. (12) and (13) into Eq. (5), we obtain the waveguide analog of Eq. (6) for large r:

$$P_s(\mathbf{x}) \sim D(\theta)G(\mathbf{x},\mathbf{x}_0), \tag{14}$$

where

$$D(\theta) = -\frac{1}{4\pi}\int\int_{\partial\Gamma}\left(ik_0\hat{n}\cdot\hat{r}P(\mathbf{x}') + \frac{\partial P}{\partial n}(\mathbf{x}')\right) \times \exp(-ik_0\mathbf{x}'\cdot\hat{r})dA'. \tag{15}$$

Thus the scattered field can be approximated by a specular-point-source field for $r \gg L$. This result, which was obtained for a rigid sphere in Ref. 5, is in agreement with some observations for multipole sources.[22] Since Eq. (14) is a leading-order approximation, it should be most accurate in the forward and specular scattering directions, where P_s is most intense. In other directions, P_s is relatively weak, and higher-order asymptotic terms may be important.

II. THE MATCHED ASYMPTOTIC SOLUTION

The matched asymptotic solution of a differential equation is composed of the inner solution, which is valid in the inner region of the domain, and the outer solution, which is valid in the outer region of the domain (sometimes an intermediate region is required). Different terms of the differential equation are important in the two regions. For example, we consider the matched asymptotic solution of Eq. (3). A leading-order inner solution is obtained by assuming that the

inner region near Ω is homogeneous with $c = c_0$ and $\beta = 0$ (Ref. 17). In the outer region far from Ω ($k_0 r \gg 1$), the asymptotic expression for the Hankel functions appearing in the normal mode solution[23,24] of Eq. (3) is valid. Thus Eq. (3) may be replaced with the PE in the outer region.

If the inner and outer regions overlap, the following matched asymptotic solution of Eq. (3) is obtained:

$$G \sim \begin{cases} G_{\text{in}} & r < r_0, \\ G_{\text{out}} & r > r_0, \end{cases} \tag{16}$$

where $r_0 < r_c$ (Ref. 17). The inner solution G_{in} is the homogeneous half-space Green's function, which satisfies the pressure release boundary condition at $z = 0$, the outgoing radiation condition at infinity, and

$$\nabla^2 G_{\text{in}} + k_0^2 G_{\text{in}} = -4\pi\delta(\mathbf{x} - \mathbf{x}'), \tag{17}$$

$$G_{\text{in}}(\mathbf{x},\mathbf{x}') = G_f(\mathbf{x},\mathbf{x}') - G_f(\mathbf{x}_*,\mathbf{x}'), \tag{18}$$

$$\mathbf{x}_* = (x, y, -z). \tag{19}$$

For many problems, G_{in} excites the propagating normal modes more accurately than the Gaussian PE starter.[17] Although G_{in} breaks down for $k_0(z - d) \gg 1$, this does not affect the accuracy of G_{out} because rays that enter the sediment in the inner region are not trapped. In the outer region $r > r_0$, the outer solution satisfies

$$\rho\nabla\cdot\left(\frac{1}{\rho}\nabla G_{\text{out}}\right) + K^2 G_{\text{out}} = 0, \tag{20}$$

with the boundary condition $G_{\text{out}} = G_{\text{in}}$ at $r = r_0$. The PE can be used to solve Eq. (20) if $k_0 r_0 \gg 1$.

Treating the region near a point source as a lossless, homogeneous half-space causes negligible errors in the far-field because refraction in the ocean is weak, attenuation in the ocean bottom is weak, and rays that reflect from the ocean bottom near the source propagate at large vertical angles and are not trapped by the oceanic waveguide. Since Γ behaves like a collection of point sources, one would expect that an analogous matched asymptotic solution that involves the solution of the half-space scattering problem exists for the waveguide scattering problem.

The waveguide scattering problem can be posed as an integral equation involving G. We do not write down the integral equation because its form depends on the properties of Γ. An asymptotic solution of the integral equation is obtained by approximating G with G_{in} on $\partial\Gamma$, which gives the integral equation for the homogeneous half-space scattering problem having the solution $(P_s)_{\text{in}}$ with the total field P_{in}. This approach is an alternative to the Kirchhoff method, which is used to solve scattering integral equations by approximating P on $\partial\Gamma$. Thus we obtain the following matched asymptotic solution for P_s:

$$P_s \sim \begin{cases} (P_s)_{\text{in}} & r < r_0, \\ (P_s)_{\text{out}} & r > r_0, \end{cases} \tag{21}$$

$$\rho\nabla\cdot\left(\frac{1}{\rho}\nabla(P_s)_{\text{out}}\right) + K^2 (P_s)_{\text{out}} = 0, \tag{22}$$

with the boundary condition $(P_s)_{\text{out}} = (P_s)_{\text{in}}$ at $r = r_0$. The PE can be used to solve Eq. (22) if $k_0 r_0 \gg 1$. Decoupling the waveguide scattering problem is a useful simplification because models for solving the half-space scattering problem and the propagation problem in the outer region have been developed.

The matched asymptotic solution for a point source is very accurate in the outer region,[17] and Γ behaves like a collection of point sources. Unlike a point source, however, Γ can induce multiple reflections between itself and the ocean surface and bottom. The matched asymptotic solution accounts for multiple reflections between Γ and the ocean surface. Unless Γ is very close to the ocean bottom, rays that travel between two points on $\partial\Gamma$ via bottom reflection meet the ocean bottom at nearly normal incidence for which the reflection coefficient is small. Furthermore, many of the rays involved in multiple reflections between Γ and the ocean bottom propagate away from Γ with large angles and are not trapped within the water column. Thus the matched asymptotic solution for P_s should be very accurate in the outer region.

Although $(P_s)_{\text{in}}$ breaks down for $k_0(z - d) \gg 1$, the following asymptotic solution is valid for $k_0(z - d) \gg 1$:

$$P_s(\mathbf{x}) \sim \frac{1}{4\pi}\int_{\partial\Gamma}\int\left(\frac{\partial G}{\partial n}(\mathbf{x},\mathbf{x}')P_{\text{in}}(\mathbf{x}') - \frac{\partial P_{\text{in}}}{\partial n}(\mathbf{x}')G(\mathbf{x},\mathbf{x}')\right)dA'. \tag{23}$$

Since the waveguide Green's function is used in Eq. (23), this representation accounts for refraction, reflection, and attenuation in the region $r < r_0$. Since Eq. (16) is very accurage in the outer region, however, it is not beneficial to use Eq. (23) in the outer region.

Let us outline the sequence of steps involved in the solution of scattering problems with the model. The incident field is computed with a propagation model such as the PE. The 3DPE must be used if azimuthal diffraction is important. A scattering model is then used to compute $(P_s)_{\text{in}}$ at $r = r_0$. Since the accuracy of $(P_s)_{\text{in}}$ improves as r_0 decreases, it is desirable to choose r_0 as small as possible. Since many scattering models assume an incident plane wave, it may be useful to use the waveguide normal modes to decompose P_i into plane waves as discussed in Ref. 5. Although the half-space scattering problem is much easier than the waveguide scattering problem, it is more difficult than the free-space scattering problem. Multiple reflections between Γ and the ocean surface give rise to mostly wide-angle rays if Γ is not too close to the ocean surface. Thus multiple reflections may be ignored if z_0 is sufficiently large. This aproximation, which was used in Ref. 5, is equivalent to imaging the free-space scattered field to obtain

$$(P_s)_{\text{in}}(\mathbf{x}) \cong (P_s)_f(\mathbf{x}) - (P_s)_f(\mathbf{x}_*). \tag{24}$$

A propagation model is used to solve the outer problem for $r > r_0$. The PE may be used if $k_0 r_0 \gg 1$. The 3DPE is required, in general, because P_s and possibly c, ρ, and β depend on θ. In stratified environments, however, azimuthal diffraction diminishes rapidly with range, and the 3DPE is required only in the intermediate region $r_0 < r < r_1$. The 2DPE is valid for $r > r_1$.

III. LOW-FREQUENCY APPROXIMATIONS

For the remaining discussion, we assume that $k_0L = O(1)$. The results in the remaining sections are valid for scatterers of arbitrary composition, shape, location, and orientation. For the examples, however, Γ is taken to be a rigid spheroid of length L and girth πB, where $k_0B = O(1)$, with its major axis parallel to the x axis. Since Ω is far from Γ and range and azimuth variations are weak, the PE can be used to compute

$$P_i = U_i(r',z,\theta')\exp(ik_0r'), \tag{25}$$

where r' is the horizontal distance from Ω and θ' is the azimuth angle about Ω. Far from Ω, $\partial U_i/\partial r' = O(k_0\epsilon)$, $\partial U_i/\partial z = O(k_0\epsilon^{1/2})$, and $\partial U_i/\partial\theta' \ll k_0r'$ (Ref. 8). Thus P_i can be approximated to leading order on $\partial\Gamma$ by a plane wave

$$P_i \sim U_i(r_i,z_0,\theta_i + \pi) \times \exp[ik_0(r_i - x\cos\theta_i - y\sin\theta_i)]. \tag{26}$$

This is a useful approximation because many scattering models assume an incident plane wave. If $B \ll L$, the accuracy of Eq. (26) depends on the orientation of Γ. Higher frequencies are permitted for broadside incidence than for end-on incidence.

A standard approach for matching the inner and outer solutions of a matched asymptotic solution is to consider the outer expansion of the inner solution.[25] For trapped rays, $D_f(\theta,\phi) \sim D_f(\theta,0)$ in the limit $\epsilon \to 0$. Thus we use Eq. (6) with $\phi = 0$ and Eqs. (18) and (24) to obtain the outer expansion of $(P_s)_{in}$:

$$(P_s)_{in}^{out} = U_i(r_i,z_0,\theta_i + \pi)\exp(ik_0r_i)D_f(\theta,0) \times G_{in}(\mathbf{x},\mathbf{x}_0). \tag{27}$$

For the case $r_1 = r_0$ (no intermediate region required), we use the fact that $G_{in}^{out} = G_{in}$ and the matching principle[25] to obtain the specular-point-source approximation

$$(P_s)_{out} = P_i(r_i,z_0,\theta_i + \pi)D_f(\theta,0)G(\mathbf{x},\mathbf{x}_0). \tag{28}$$

This approximation produces a significant gain in efficiency because D_f, which is difficult to compute, appears in Eq. (28) only for $\phi = 0$. We deduce that $D(\theta) \propto D_f(\theta,0)$.

To investigate the accuracy of Eq. (28), we consider the problem described in Table I, where subscripts w and b denote water and bottom values. The free-space radiation pattern $20\log_{10}|D_f(\theta,0)|$ appears in Fig. 2 for large r and for $r = r_c$. Since the radiation pattern has nearly settled down at $r = r_c$, Eq. (28) should be a good approximation for this problem. Since r_0 is substantially less than r_c, Eq. (16) is very accurate. However, it is apparent from Fig. 3 that the free-space radiation pattern at $r = r_0$ has not settled down. Thus we use the 3DPE for $r_0 < r < r_1$.

TABLE I. Data for the frequency-domain problem.

$\omega = 200\pi$ s^{-1}	$d = 225$ m	$c_b = 1500$ m/s
$c_w = 1600$ m/s	$\rho_b = 1.5$ g/cm^3	$\beta_b = 0.5$ dB/λ
$L = 50$ m	$B = 10$ m	$\phi_c = 20.4°$
$r_c = 202.1$ m	$r_1 = 1000$ m	$r_0 = 75$ m
$z_0 = 150$ m	$r_s = 5$ km	$z_s = 50$ m
$\theta_i = 135°$	$z_r = 50$ m	

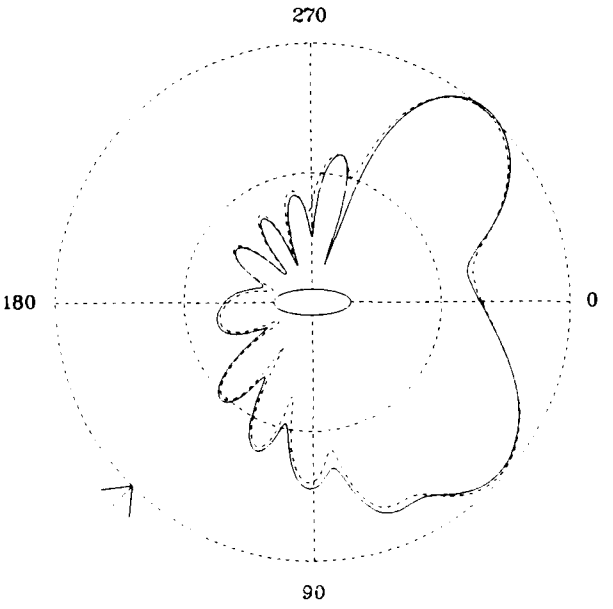

FIG. 2. The free-space radiation pattern at $r = r_c$ (solid curve) and for large r (dashed curve).

We used Eq. (26) to simplify P_i to a plane wave and Eq. (24) and the T-matrix method[26,27] to compute D_f and $(P_s)_{in}$. Transmission loss for P_i and P_s computed with Eq. (28) and with the PE using $(P_s)_{in}$ as an initial condition appears in Fig. 4. From the data in Table II, we observe that the approximation $D_f(\theta,\phi) \cong D_f(\theta,0)$ is not accurate for $\phi < \phi_c$ in the directions $\theta = 0°$, 180° and 225°. This explains the differences in the solutions for P_s appearing in Fig. 4 for these directions. The solutions are in excellent agreement in the other directions including the forward and specular directions.

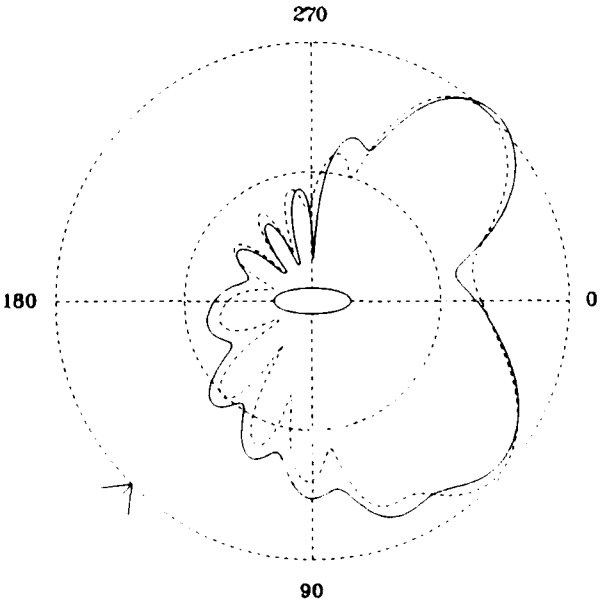

FIG. 3. The free-space radiation pattern at $r = r_0$ (solid curve) and for large r (dashed curve).

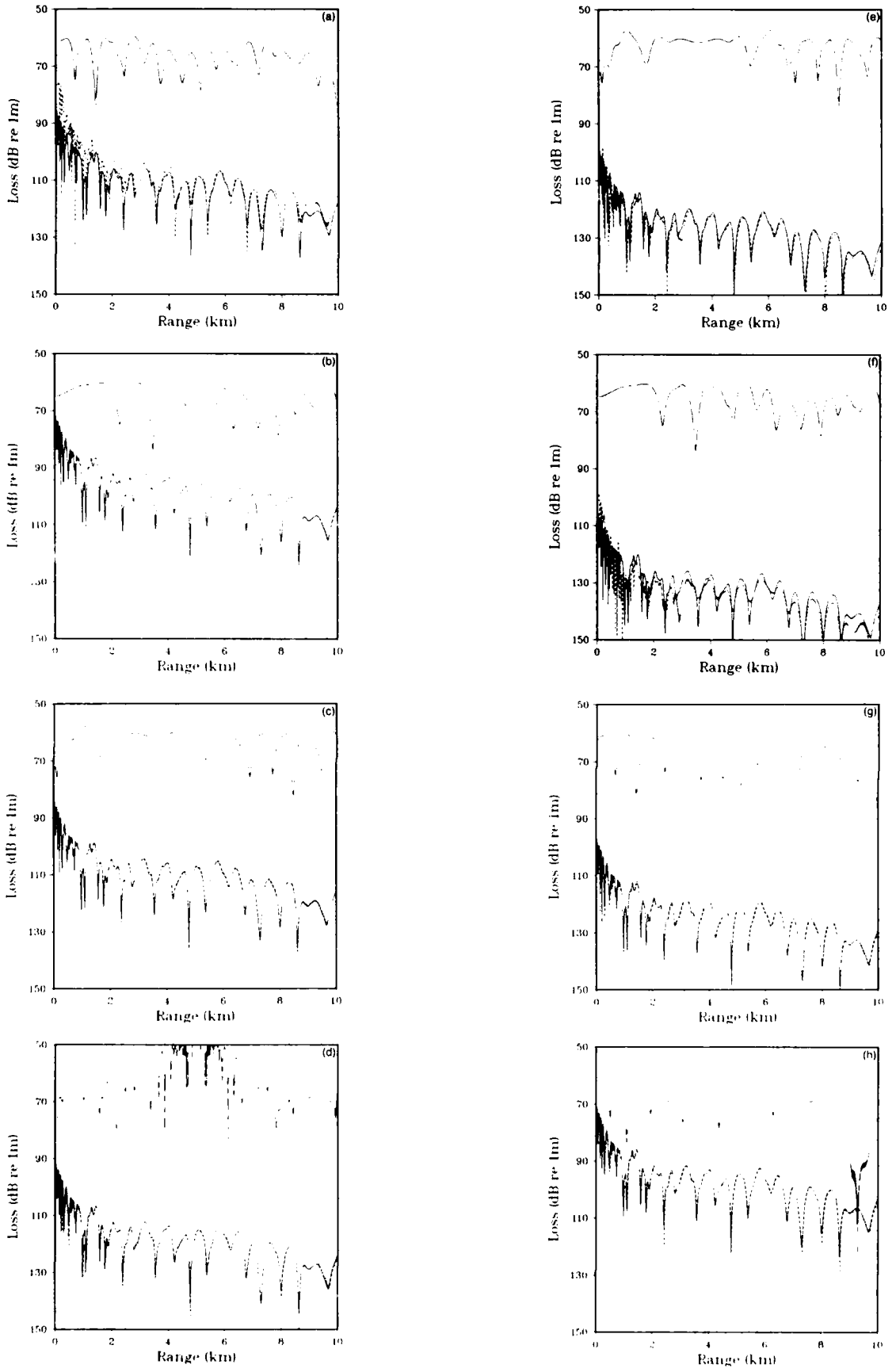

FIG. 4. The specular-point-source approximation (solid curves), the full matched asymptotic solution involving PE calculations (dashed curves), and the incident field (broken curves) for: (a) $\theta_0 = 0°$; (b) $\theta_0 = 45°$; (c) $\theta_0 = 90°$; (d) $\theta_0 = 135°$; (e) $\theta_0 = 180°$; (f) $\theta_0 = 225°$; (g) $\theta_0 = 270°$; and (h) $\theta_0 = 315°$.

TABLE II. Behavior of $20 \log_{10}|D_f(\theta,\phi)|$.

	$\phi = 0°$	$\phi = 5°$	$\phi = 10°$	$\phi = 15°$	$\phi = 20°$
$\theta = 0°$	11.69	12.14	13.40	15.27	17.50
$\theta = 45°$	25.68	25.70	25.75	25.80	25.78
$\theta = 90°$	13.12	13.08	12.96	12.76	12.48
$\theta = 135°$	5.37	5.35	5.25	4.95	4.23
$\theta = 180°$	− 2.07	− 2.27	− 2.93	− 4.32	− 6.72
$\theta = 225°$	− 8.15	− 8.68	− 10.49	− 14.67	− 20.07
$\theta = 270°$	− 0.06	− 0.04	0.02	0.10	0.20
$\theta = 315°$	26.15	26.03	25.68	25.11	24.35

The following asymptotic expression is valid in a stratified environment for $k_0 r \gg 1$:

$$P_s \sim \pi i \sum_n E_n(\theta)\psi_n(z_0)\psi_n(z)H_0^{(1)}(k_n r), \tag{29}$$

where $E_n = D$ if Eq. (14) holds. The normal modes ψ_n and eigenvalues k_n are defined in Refs. 23 and 24. We define the modal radiation pattern associated with ψ_n to be $20 \log_{10}|E_n(\theta)|$. For the stratified environment described in Table I, modes 1, 3, 6, and 10 propagate with angles of approximately 1.82°, 5.48°, 11.04°, and 18.62°. The radiation patterns for these modes at $r = r_1$ appear in Fig. 5 with the far free-space radiation pattern. The agreement with the free-space pattern, which is excellent for mode 1, decreases with mode number. This is consistent with the small-angle asymptotics.

IV. LOW-FREQUENCY PULSE SCATTERING

To derive a matched asymptotic solution for pulsed sources, the Fourier transform is inverted in Eq. (27). The

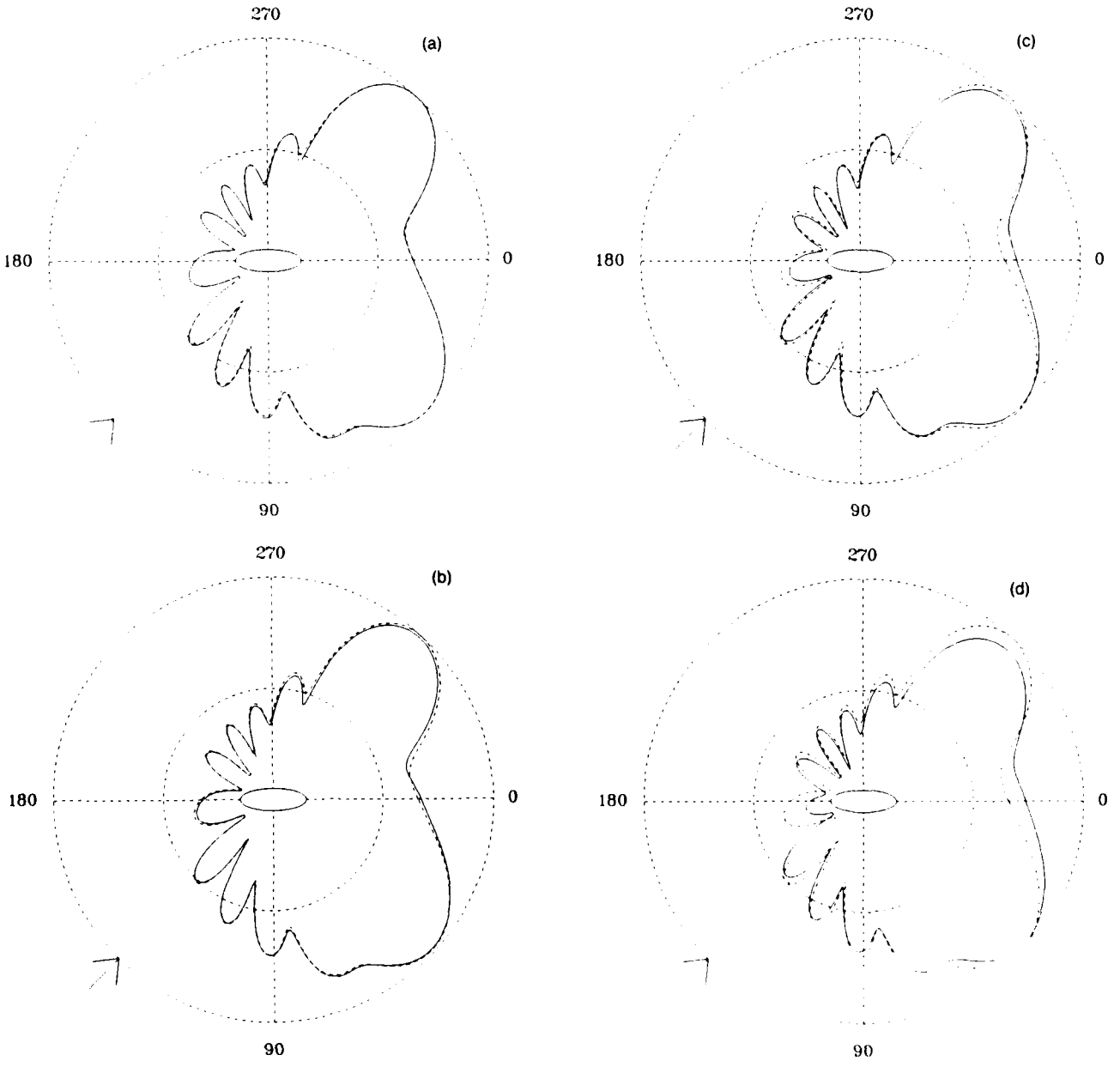

FIG. 5. The far free-space radiation pattern (dashed curves) and the modal radiation patterns (solid curves) for (a) mode 1, (b) mode 3, (c) mode 6, and (d) mode 10.

TABLE III. Data for the time-domain problem.

$\omega = 50\pi\ \mathrm{s}^{-1}$	$d = 250$ m	$c_a = 1500$ m/s
$c_b = 1600$ m/s	$\rho_b = 1.5$ g/cm^3	$\beta_b = 0.5$ dB/λ
$L = 50$ m	$B = 10$ m	$\phi_s = 20.4°$
$r_s = 268.8$ m	$r_0 = 100$ m	$z_0 = 150$ m
$r_r = 10$ km	$z_r = 25$ m	$\theta_r = 135°$
$\theta_r = 45°$		

TDPE can be used to compute the quantity $u_t(r',z,\theta',t) = p_t(r',z,\theta',t + r'/c_0)$, where

$$U_t(r',z,\theta') = \frac{1}{2\pi}\int_{-\infty}^{\infty} u_t(r',z,\theta',t)\exp(i\omega t)\,dt, \quad (30)$$

and p_t is the incident field. Since $k_0 L = O(1)$, we assume a finite bandwidth $\omega_1 < \omega < \omega_2$ and invert the Fourier transform in Eq. (27) to obtain

$$(p_s)_{\mathrm{in}}^{\mathrm{out}} = \int_{\omega_1}^{\omega_2} U_t(r_r,z_0,\theta_r + \pi)D_f(\theta,0) \times G_{\mathrm{in}}(\mathbf{x},\mathbf{x}_0)\exp[-i\omega(t - r_r/c_0)]\,d\omega. \quad (31)$$

We substitute Eq. (30) into Eq. (31) and interchange the order of integration to obtain

$$(p_s)_{\mathrm{in}}^{\mathrm{out}} = \frac{1}{d_-}F\left(\theta,t - \frac{d_- + r_r}{c_0}\right) - \frac{1}{d_+}F\left(\theta,t - \frac{d_+ + r_r}{c_0}\right), \quad (32)$$

$$d_\pm^2 = r_r^2 + (z \pm z_0)^2, \quad (33)$$

$$F(\theta,t) = \int_{-\infty}^{\infty} K(\theta,t - t')u_t(r_r,z_0,\theta_r + \pi,t')\,dt', \quad (34)$$

$$K(\theta,t) = \frac{1}{2\pi}\int_{\omega_1}^{\omega_2} D_f(\theta,0)\exp(-i\omega t)\,d\omega. \quad (35)$$

The integral operator in Eq. (34) transforms incident waveforms into scattered waveforms. If Eq. (28) is valid, $(p_s)_{\mathrm{in}}^{\mathrm{out}}$ may be used to initialize the TDPE at $r = r_0 < r_c$.

To illustrate the time-domain solution, we consider the Hanning weighted sinusoidal source function[28]

$$f(t) = \begin{cases} (1 - \cos\tfrac{1}{4}\omega t)\sin\omega t, & 0 < t < T, \\ 0, & \text{otherwise}, \end{cases} \quad (36)$$

where $\omega = 50\pi s^{-1}$ and $T = 8\pi/\omega$, and an example for which data appear in Table III. The incident field p_t computed with the TDPE appears in Fig. 6. The ocean bottom is marked with a horizontal line. The solid contours correspond to $p_t > 0$; the dashed contours correspond to $p_t < 0$. Although the time-dependent wave equation does not separate in depth since c depends on z, normal mode structure is visible in Fig. 6. The first mode is present near $t = 150$ ms, the second mode near $t = 250$ ms, and the third mode near $t = 400$ ms. We used the T-matrix method to calculate D_f. The incident waveform $u_t(r_r,z_0,\theta_r + \pi,t)$ and the scattered waveform $F(\theta_r,t)$ appear in Fig. 7. Equation (32) was used to calculate $(p_s)_{\mathrm{in}}^{\mathrm{out}}$, which appears in Fig. 8.

The TDPE was applied in the specular direction to obtain the scattered field $(p_s)_{\mathrm{out}}$, which appears in Fig. 9. Normal mode structure is also visible in $(p_s)_{\mathrm{out}}$. However, the second mode is not excited because it vanishes near the center of Γ. Furthermore, the arrival times of the modes in the scattered field are qualitatively different from the arrival times of the modes in the incident field because the scattering process redistributes the energy among the modes.[5] In contrast to the incident field, the first mode arrives twice, near $t = 200$ ms and near $t = 400$ ms. The third-mode arrivals behave similarly. Furthermore, the arrival times of the first and third modes overlap.

V. CONCLUSIONS

A matched asymptotic solution has been derived for underwater acoustics problems involving both propagation and scattering. The propagation and scattering aspects of the

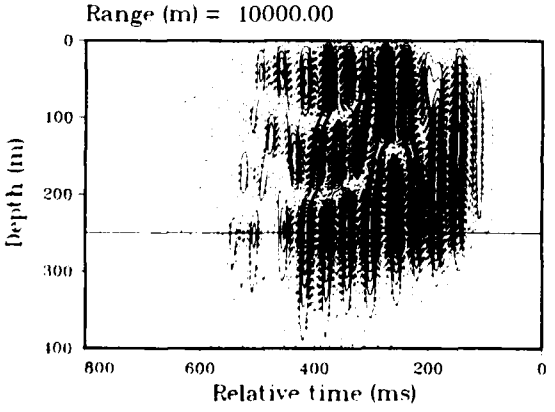

FIG. 6. The incident pulse. Patterns of the first three normal modes are clearly visible.

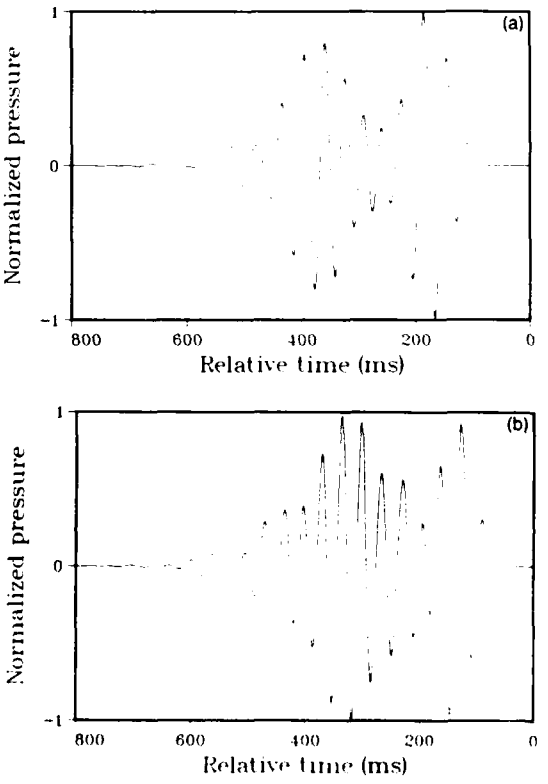

FIG. 7. The waveforms: (a) incident and (b) scattered

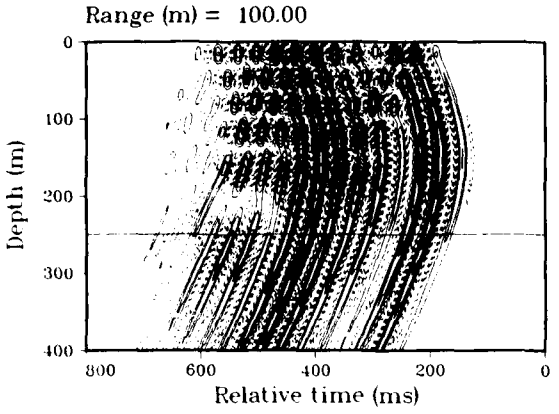

FIG. 8. The half-space scattered field $(p_s)_m^{out}$ at $r = 100$ m in the specular direction $\theta_s = 45°$.

problem are decoupled. The model is valid for scatterers of arbitrary geometry and composition in three-dimensional environments. Since the small-angle limit has been used, the model is efficient and accurate. In its most general form, the model requires the solution of the half-space scattering problem and the 3DPE. If the scatterer is far from the ocean surface, however, the half-space scattering problem can be replaced with the free-space scattering problem. If the scatterer is far from the ocean bottom, the solution of the 3DPE is not required because the inner region extends to a relatively large range. For low frequencies, the incident field can be approximated by a plane wave, and the scattered field can be approximated by the field due to an azimuthally specular point source. These approximations make low-frequency pulse scattering problems practical.

ACKNOWLEDGMENTS

This work was supported by the Office of Naval Research and the Naval Ocean Research and Development Activity. M. D. Collins thanks G. A. Kriegsmann and E. L. Reiss for supporting this work as part of a dissertation at Northwestern University.

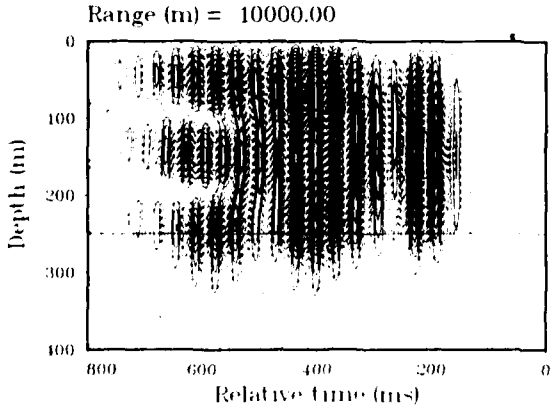

FIG. 9. The waveguide scattered field $(p_s)_{\ldots}$ at $r = 10$ km in the specular direction $\theta_s = 45°$. Partially overlapping patterns of the first and third modes are visible.

[1] D. S. Ahluwalia and J. B. Keller, "Exact and Asymptotic Representations of the Sound Field in a Stratified Ocean," in *Wave Propagation and Underwater Acoustics*, edited by J. B. Keller and J. S. Papadakis, Vol. 70 of *Lecture Notes in Physics* (Springer, New York, 1977).

[2] *Acoustic, Electromagnetic, and Elastic Wave Scattering - Focus on the T-Matrix Approach*, edited by V. K. Varadan and V. V. Varadan (Pergamon, New York, 1980).

[3] A. Boström, "Transmission and Reflection of Acoustic Waves by an Obstacle in a Waveguide," Wave Motion **2**, 167–184 (1984).

[4] R. H. Hackman and G. S. Sammelmann, "Acoustic Scattering in an Inhomogeneous Waveguide: Theory," J. Acoust. Soc. Am. **80**, 1447–1458 (1986).

[5] F. Ingenito, "Scattering from an Object in a Stratified Medium," J. Acoust. Soc. Am. **82**, 2051–2059 (1987).

[6] F. D. Tappert, "The Parabolic Approximation Method," in *Wave Propagation and Underwater Acoustics*, edited by J. B. Keller and J. S. Papadakis, Vol. 70 of *Lecture Notes in Physics* (Springer, New York, 1977).

R. N. Baer, "Propagation through a Three-Dimensional Eddy Including Effects on an Array," J. Acoust. Soc. Am. **69**, 70–75 (1981).

[8] W. L. Siegmann, G. A. Kriegsmann, and D. Lee, "A Wide-Angle Three-Dimensional Parabolic Wave Equation," J. Acoust. Soc. Am. **78**, 659–664 (1985).

[9] D. Lee, Y. Saad, and M. H. Schultz, "An Efficient Method for Solving the Three-Dimensional Wide Angle Wave Equation," Yale University Research Rep. YALEU/DCS/RR-463 (1986).

[10] J. S. Perkins and R. N. Baer, "An Approximation to the Three-Dimensional Parabolic-Equation Method for Acoustic Propagation," J. Acoust. Soc. Am. **72**, 515–522 (1982).

[11] J. F. Claerbout and A. G. Johnson, "Extrapolation of Time Dependent Waveforms Along Their Path of Propagation," Geophys. J. R. Astron. Soc. **26**, 285–295 (1971).

[12] J. E. Murphy, "Finite-Difference Treatment of a Time-Domain Parabolic Equation: Theory," J. Acoust. Soc. Am. **77**, 1958–1960 (1985).

[13] B. E. McDonald and W. A. Kuperman, "Time Domain Formulation for Pulse Propagation Including Nonlinear Behavior at a Caustic," J. Acoust. Soc. Am. **81**, 1406–1417 (1987).

[14] M. D. Collins, "Low-Frequency, Bottom-Interacting Pulse Propagation in Range-Dependent Oceans," IEEE J. Ocean. Eng. **13**(4), 222–228 (1988).

[15] M. D. Collins, "The Time-Domain Solution of the Wide-Angle Parabolic Equation Including the Effects of Sediment Dispersion," J. Acoust. Soc. Am. **84**, 2114–2125 (1988).

[16] M. D. Collins, "Applications and Time-Domain Solution of Higher-Order Parabolic Equations in Underwater Acoustics," J. Acoust. Soc. Am. (submitted).

[17] M. D. Collins, "A Nearfield Asymptotic Analysis for Underwater Acoustics," J. Acoust. Soc. Am. **85**, 1107–1114 (1989).

[18] C. M. Bender and S. A. Orszag, *Advanced Mathematical Methods for Scientists and Engineers* (McGraw-Hill, New York, 1978), pp. 417–483.

[19] P. G. Bergmann, "The Wave Equation in a Medium with a Variable Index of Refraction," J. Acoust. Soc. Am. **17**, 329–333 (1946).

[20] E. L. Hamilton, "Compressional-Wave Attenuation in Marine Sediments," Geophysics **37**, 620–646 (1972).

[21] N. Bleistein and R. A. Handelsman, *Asymptotic Expansions of Integrals* (Dover, New York, 1986), pp. 55–60.

A. J. Haug, R. D. Graves, and H. Uberall, "Normal-Mode Theory of Underwater Sound Propagation from Stationary Multipole Sources: Results for a Realistic Sound-Speed Profile," J. Acoust. Soc. Am. **57**, 1052–1061 (1975).

[23] R. B. Evans, "A Coupled-Mode Solution for Acoustic Propagation in a Waveguide with Stepwise Depth Variations of a Penetrable Bottom," J. Acoust. Soc. Am. **74**, 188–195 (1983).

[24] A. D. Pierce, "Augmented Adiabatic Mode Theory for Upslope Propagation for a Point Source in Variable-Depth Shallow Water Overlying a Fluid Bottom," J. Acoust. Soc. Am. **74**, 1837–1847 (1983).

A. H. Nayfeh, *Introduction to Perturbation Techniques* (Wiley, New York, 1981), pp. 265–268.

[26] P. C. Waterman, "New Foundation of Acoustic Scattering," J. Acoust. Soc. Am. **45**, 1417–1429 (1969).

M. F. Werby and S. A. Chin-Bing, "Some Numerical Techniques and Their Use in the Extension of T-Matrix and Null-Field Approaches in Scattering," Comp. Math. Appls. **11**, 717–731 (1985).

H. Schmidt, "SAFARI User's Guide," SACLANT Undersea Research Centre, La Spezia, Italy (1988).